



Stability evaluation of rock slope based on discrete fracture network and discrete element model: a case study for the right bank of Yigong Zangbu Bridge

Yuchao Li¹ · Jianping Chen¹ · Fujun Zhou² · Yiding Bao³ · Zhihai Li¹ · Shengyuan Song¹ · Chen Cao¹

Received: 2 May 2021 / Accepted: 26 September 2021 / Published online: 8 October 2021
© The Author(s), under exclusive licence to Springer-Verlag GmbH Germany, part of Springer Nature 2021

Abstract

Distribution characteristics and strength of 3D discrete fractures have a decisive effect on the rock slope stability. How to use the fractures obtained on site to establish a 3D fractured rock slope for stability analysis is a difficult problem in the field of rock mass engineering. This study selected the rock slope on the right bank of Yigong Zangbu Bridge for a detailed field investigation. Exposed joints and fractures were measured and counted. Occurrence, size, and position distribution models of the fractures were used to obtain the parameters of the spatial distribution using probability and statistic theory. Then, a complex 3D discrete fracture network (DFN) was established and simplified. After that, a 3D rock slope model was built and the DFN was used to cut the slope model. Finally, the strength reduction method was used to analyze the slope stability. The results reveal that the overall slope stability is good (safety factor is 2.0), but the local block deformations are large and are mainly concentrated in the lower part of the slope. Due to the existence of structural planes dipping outside the slope on the right bank, local unstable blocks are easily formed. In this study, the whole process from field fracture acquisition to the DFN generation is applied to the 3D fracture rock slope stability analysis, which is of great importance for complex rock mass engineering assessment and disaster prevention.

Keywords Discrete element model · 3D fracture network model · Jointed rock slope · Probability model · Stability analysis

1 Introduction

Due to the existence of fissures, the rock mass has typical discontinuous, heterogeneous, and anisotropic characteristics. This has a significant influence on the mechanical and hydraulic properties of the rock mass [23, 24, 57]. It is accepted that the stability of rock slopes depends on the

distribution and strength of joints and cracks. Therefore, determining the characteristics of occurrence distribution, trace length, and spacing is important for the stability evaluation [16]. However, it is difficult to obtain real information due to the randomness, complexity, and invisibility of joints and fissures [56]. The discrete fracture network (DFN) model based on probability statistics is considered a suitable method that reflects the characteristics of fractures in rock masses [41]. The DFN model mainly consists of three probability distribution models of fracture occurrence, size, and location [5, 14, 48]. On this basis, various methods for generating DFN have been proposed, such as the most typical Monte Carlo method [9, 10].

Many probability distributions are used to establish the fracture occurrence distribution model, including fisher, uniform, exponential, normal, and log-normal distribution [5, 28, 49]. Among these probability distributions, fisher

✉ Jianping Chen
chenjp@jlu.edu.cn

¹ College of Construction Engineering, Jilin University, Changchun 130026, China

² China Railway First Survey and Design Institute Group CO., LTD, Xi'an 710043, China

³ Key Laboratory of Mountain Hazards and Earth Surface Process, Institute of Mountain Hazards and Environment, Chinese Academy of Sciences (CAS), No. 9, Block 4, South Renmin Road, Chengdu 610041, China

and empirical have been widely adopted in recent years thanks to good performance in simulation and easy realization in mathematics [19]. The validity of the distribution model can be checked by the Chi-square test and the Kolmogorov–Smirnov (K–S) test [55]. However, due to measurement errors and the complexity of geological structures, it is still impossible to obtain the real occurrence of fractures in the rock mass [32].

As for obtaining the fracture size distribution, it mainly depends on the probability distribution of the measured trace length [43]. Data for the 2D fracture trace length are obtained from rock outcrop and then transformed into 3D to obtain the spatial distribution characteristics of fracture size [43, 46, 54]. Sampling and statistical biases can occur in the process of fracture collection and treatment [23, 24, 36, 52], which can be modified by some methods [29, 52]. Zhang [51] found that the coefficient of variation of the measured trace length distribution is close to the real trace length. Furthermore, the real trace length distribution type is generally considered to be the same as the measured trace length distribution [21]. Position of the fractures is also an important parameter of the DFN model. By setting up the distribution model and calculating the volume density, the fractures position can be well displayed [48].

A lot of work has been done on the analysis of rock slope stability as it represents a classical problem in geotechnical engineering. The stiffness limit equilibrium method is considered to be the main method of stability analysis in the early stage [45]. In recent years, various calculation methods and numerical methods, such as the finite element method (FEM) [27, 44, 47], the finite difference method (FDM) [6], the discrete element method (DEM) [3, 25], and the discontinuity deformation analysis (DDA) [15, 34], have been widely used. In addition, many studies use the strength reduction method (SRM) combined with FEM and FDM to analyze slope stability [1, 12, 58]. However, as a continuous numerical method, they are not suitable for the analysis of the discontinuous jointed rock slopes. Conversely, it is reasonable to adopt the discontinuous DEM for analyzing the stability and failure of discontinuous materials such as jointed rock masses [2, 35, 42]. However, this method is still not able to specifically characterize the spatial distribution of fractures in the rock mass. Therefore, a comprehensive method for the analysis of rock slope stability based on DFN and DEM is urgently needed, and this method can truly characterize the physical and mechanical properties of fractures and rock masses and reflect the stress and strain state of rock mass.

The proposed Yigong Zangbu Bridge is a significant livelihood guarantee and fundamental construction project. Therefore, it is essential to understand the potential threats to Yigong Zangbu Bridge. This paper analyzes the rock

slope stability on the right bank of the bridge. The occurrence distribution model, the size distribution model, and the position distribution model of the fractures are built on the basis of the probability and statistics theory, and the spatial distribution characteristics of fractures are obtained. Furthermore, the validity-tested DFN was established and simplified in accordance with the standard determined by the uniaxial compression test model. A 3D geomechanical model of fractured rock slope that contains a simplified DFN is established in the discrete element software 3DEC. After determining the boundary conditions and material parameters of the model, the SRM based on the catastrophe displacement criterion is applied for the analysis of the rock slopes stability. Finally, the possible failure mode and mechanism of the rock slopes in combination with block theory are discussed and a potential threat to the bridge is given and explained.

2 Background

2.1 Topography and tectonic conditions

The study area is located in the Yigong Township, Linzhi City, on the southeastern margin of the Qinghai Tibet Plateau (Fig. 1a). This area belongs to the geomorphic unit of the third level in the Himalayas–Hengduan Mountains with a typical alpine valley landform. The valley is deep and the elevation changes abruptly. The lowest elevation is 2006 m, while the highest is 6424 m (Fig. 1b). The target rock slope fluctuates from 50° to 70° (Fig. 1c). The Yigong Zangbu River in this section flows to the SW and merges with the Parlung Zangbo River.

The strata in the study area are mainly from the Mesoproterozoic Nyainqentanglha group (AnNq^a). Lithology is mainly gneiss, intercalated schist, and marble (Fig. 2). In terms of structural geology, the study area is located about 10 km northeast from an arc that is protruding northward from the Eastern Himalayan tectonic, which is part of the upper plate of the subduction zone formed during the Indian Plate subducting the Eurasian Plate. Therefore, the structural compression of rock masses is intense. In addition, the Yigong Zangbu River coincides with the regional northeastward strike-slip faults and converges with the northwestward strike-slip faults in Tongmai. Obviously, the spread of regional faults controls the direction of the Yigong Zangbu River in this section.

2.2 Rainfall characteristics

Under the influence of topography and the mountain barrier, the lower the altitude, the greater the rainfall in the study area. The warm humid air coming from the Indian

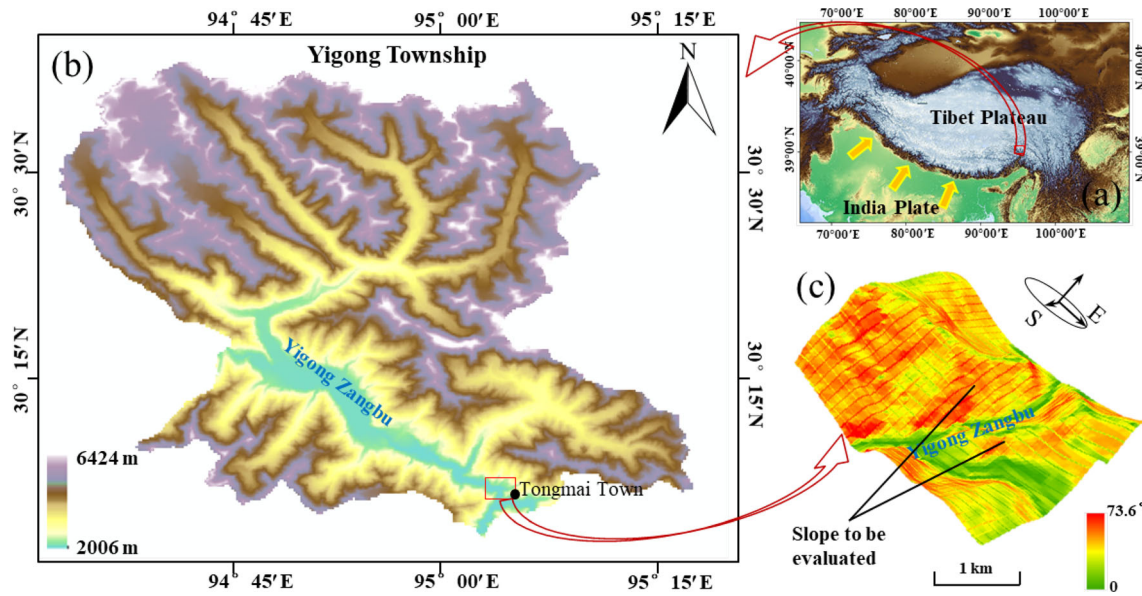


Fig. 1 Location and terrain of the study area: a Tibetan Plateau, b Yigong township, and c slope map of the rock slope

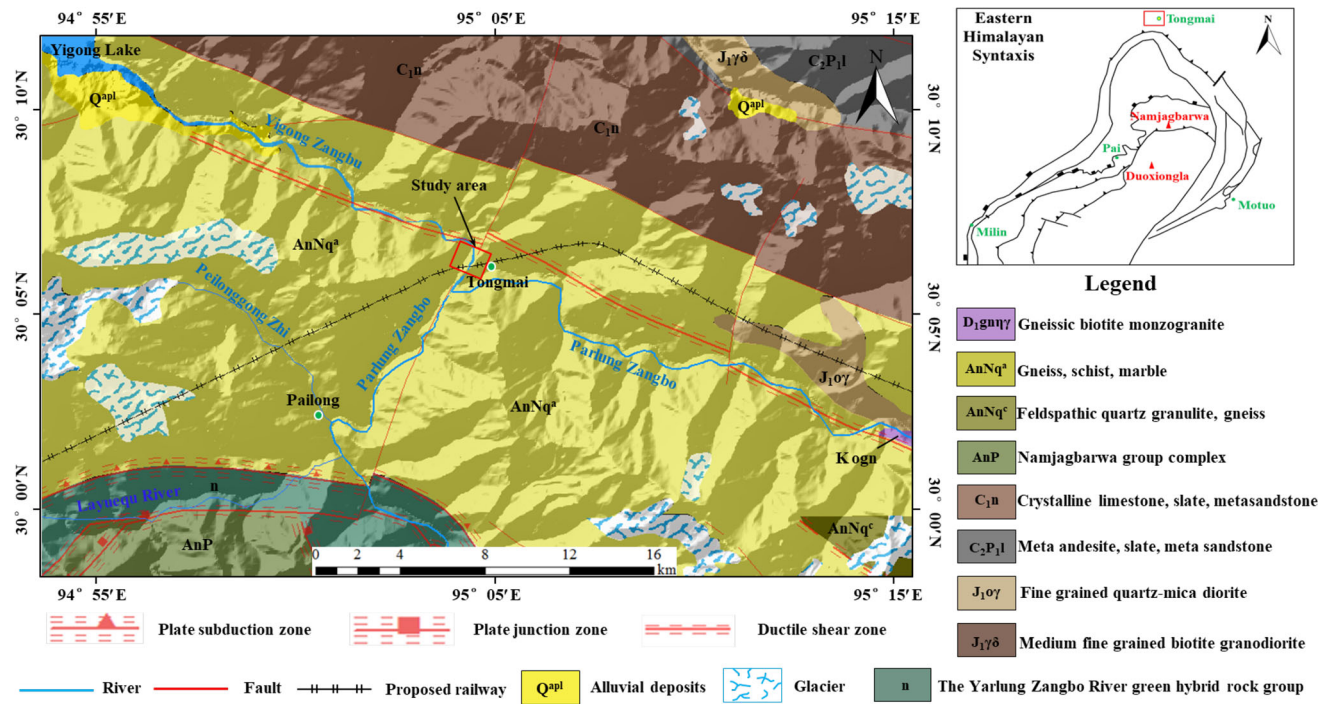


Fig. 2 Geological map of the study area

Ocean can only climb along the Yarlung Zangbo River (Fig. 3a) because of the Eastern Himalayan Syntaxis with the high peak of Namjagbarwa (7782 m). As a consequence, a special zone of rainfall distribution is formed, which coincides with the spatial distribution of rivers. Therefore, rainy and heavy rainy areas are formed in Tongmai (Fig. 3b). According to the rainfall data of Bomi meteorological station for 30 years (1981–2010), the

average perennial rainfall is 1000–1500 mm and is mainly concentrated from March to October (accounting for more than 90% of the annual rainfall) (Fig. 3c).

2.3 Seismic conditions

Tectonic activities in the study area are mainly controlled by the suture zone of the Yarlung Zangbo River. The north

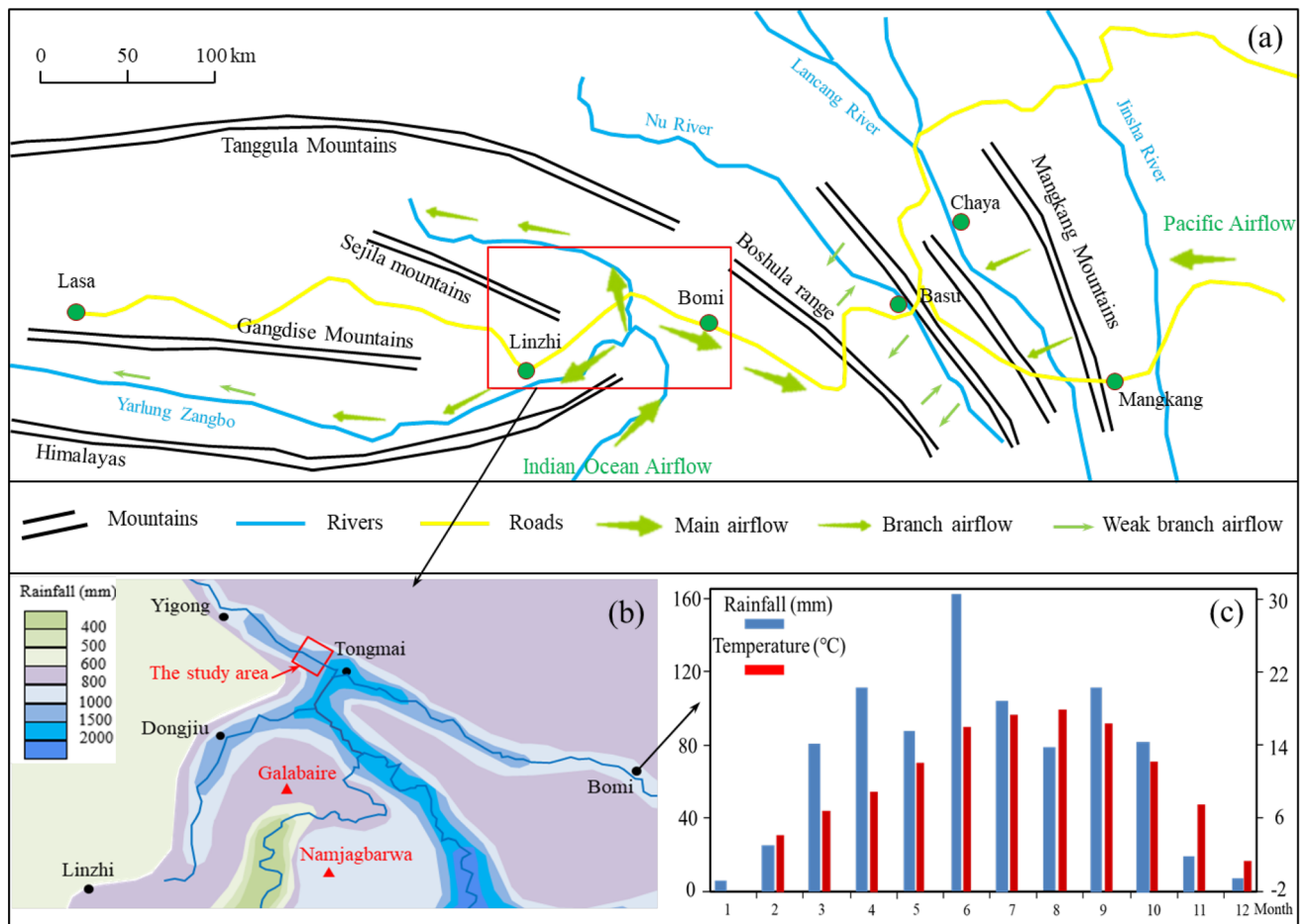


Fig. 3 Average annual rainfall zoning map of the study area and meteorological data from the Bomi Station (1981–2010)

and south sides of the suture zone are the Himalayan block and the Lhasa block, respectively, and the well-known arc-shaped Eastern Himalayan Syntaxis is also formed around Linzhi-Tongmai (Fig. 4a), which makes the area prone to earthquakes. Figure 4b shows the distribution of strong earthquakes that have occurred in recent years. The peak acceleration of ground motion in Tongmai is 0.20 g, according to the “Seismic parameter zoning map of China (GB18306-2015)” [37]. Characteristic periods of the response spectrum are 0.45 s, while the seismic intensity corresponding to the study area is IX (Fig. 4c).

2.4 Geological features

As an important part of the Sichuan–Tibet Railway in the Tongmai–Linzhi section, Yigong Zangbu Bridge spans the Yigong Zangbu River. The two ends of the bridge are connected by tunnels. The terrain of this section has a higher right and lower left bank (Fig. 5a). The entrance to the Layue Tunnel is on the right bank (Fig. 5b), while the exit from the Polong Tunnel is on the left bank (Fig. 5c). Moderately weathered gneisses are developed in a cliff-like

manner on both sides, but the slope of the left bank is gentler than the slope of the right bank. Joints and fractures are greatly developed in the bedrock due to climate and tectonic conditions. The unfavorable combination of long and large fissures on the rock slope usually constitutes unstable blocks.

A field investigation revealed more joints and fractures on the right bank (Fig. 5d). A set of large fractures inclined to the northeast at a moderate inclination angle, which is leaning toward the outside of the slope relative to the right bank. The extension scale and spacing are relatively large. Intercutting with fractures in other directions and the effect of small joints (Fig. 5e) can easily create rock masses of different sizes, which makes the situation complex. On the left bank, large fractures are leaning toward the northeast at moderate inclination angle and inclining toward the inside of the slope. In addition, there are two sets of steeply inclined structural planes that intersect the bank slope at a certain angle. These structural planes can combine and form huge rock blocks (Fig. 5f). If there is no free surface at the bottom, the block would be stationary (Fig. 5g). Because the rock slope on the right bank is more broken

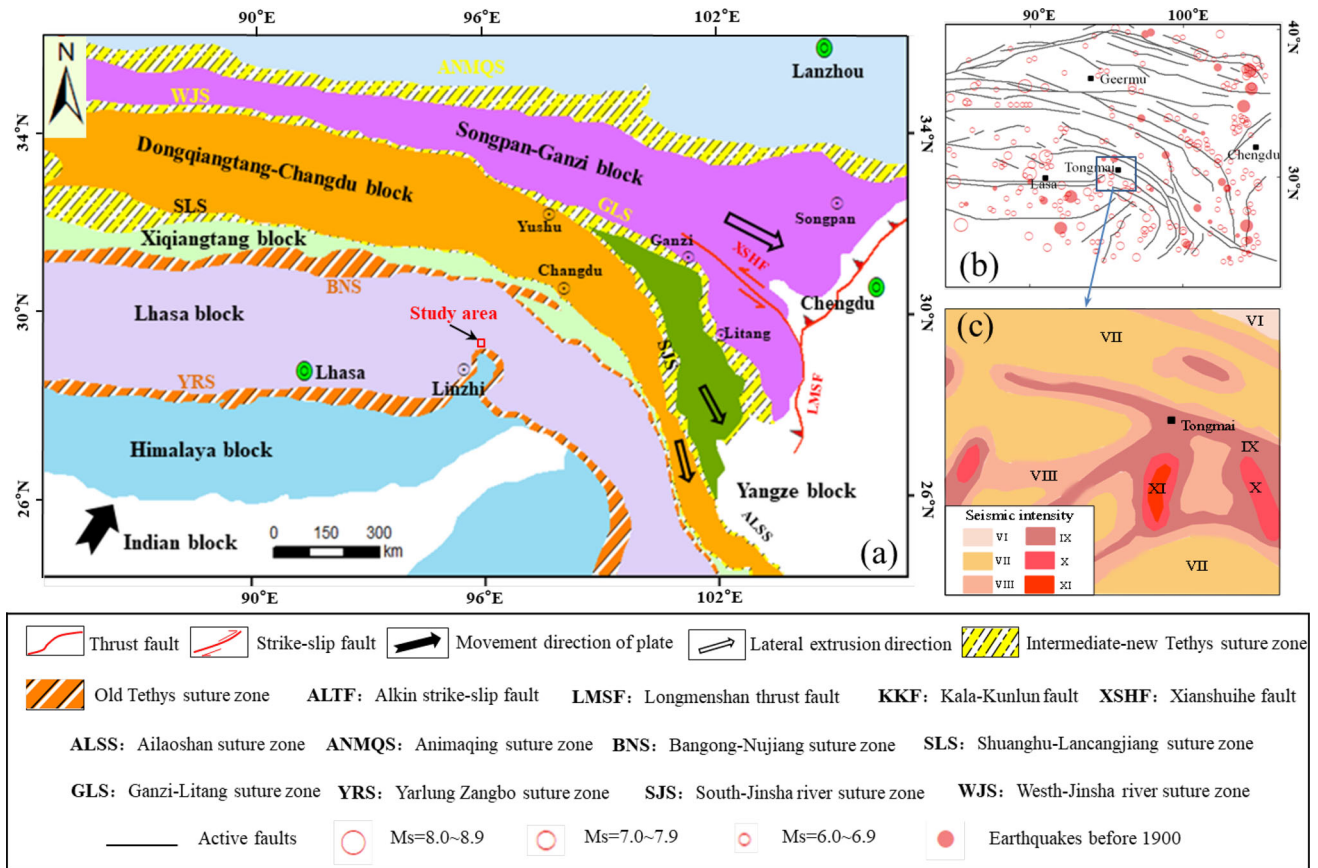


Fig. 4 a Structure outline map of the Tibetan Plateau, b active faults and earthquakes distribution, and c seismic intensity division

and the collapse already appeared, the right bank of Yigong Zangbu Bridge is taken as the object of stability evaluation in this study.

3 Method

This research is based on the probability and statistics theory, using the actual fracture data that is obtained at the site to establish a 3D DFN. Relevant parameters of the fracture distribution models are obtained and applied to subsequent modeling and stability analysis. The analysis process is shown in Fig. 6.

3.1 Data acquisition and preliminary processing

Joints and fractures data come from the adit of the right bank of the proposed bridge. The adit is about 70.5 m long, 2 m wide, and 2.35 m high. The fracture statistics window is 70 m long and 2 m high and is a relatively undisturbed and homogeneous area. A total of 67 fractures, including location, occurrence, and length are counted in the window. Figure 7 shows a two-dimensional distribution map of the investigated fractures.

According to the fracture’s direction, the “optimal vector path search method,” based on probability and statistics theory, is used to divide the structural plane superiority group [5]. The method can automatically establish vector balls on all fracture occurrence data points and measure the similarity of different fracture occurrences in the balls by giving the initial radius and step size, so as to accomplish the similarity partition of the occurrence density points. The result of partition is not unique. By estimating the objective function of each partition and comparing it with the probability distribution on the vector ball, the result of fracture grouping with the smallest objective function can be obtained. Then, each group of fractures is projected onto the Schmidt grid of the lower hemisphere. The pole map of the occurrences and the strike rose diagram of the 360° are drawn (Fig. 8). The poles distribution is random, but the structural planes that inclined to the west have a prominent advantage over the others. The characteristics of each fracture group are shown in Table 1.

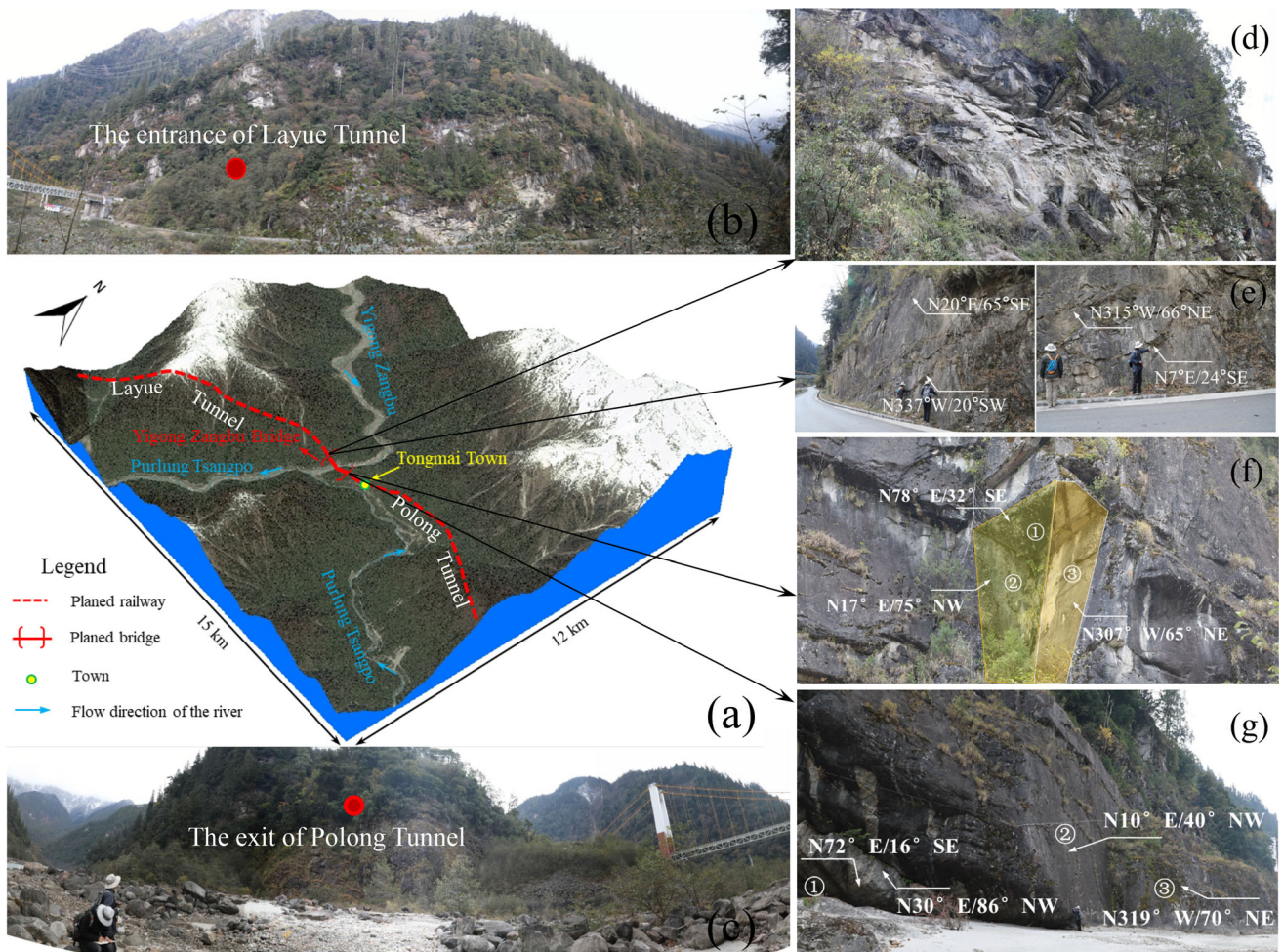


Fig. 5 **a** Three-dimensional image of the study area, **b** rock slope on the right bank of the bridge, **c** rock slope on the left bank of the bridge, **d** joints and fractures developed on the right bank, **e** occurrence of typical structural planes on the right bank, and **f** and **g** occurrence of typical structural planes on the left bank

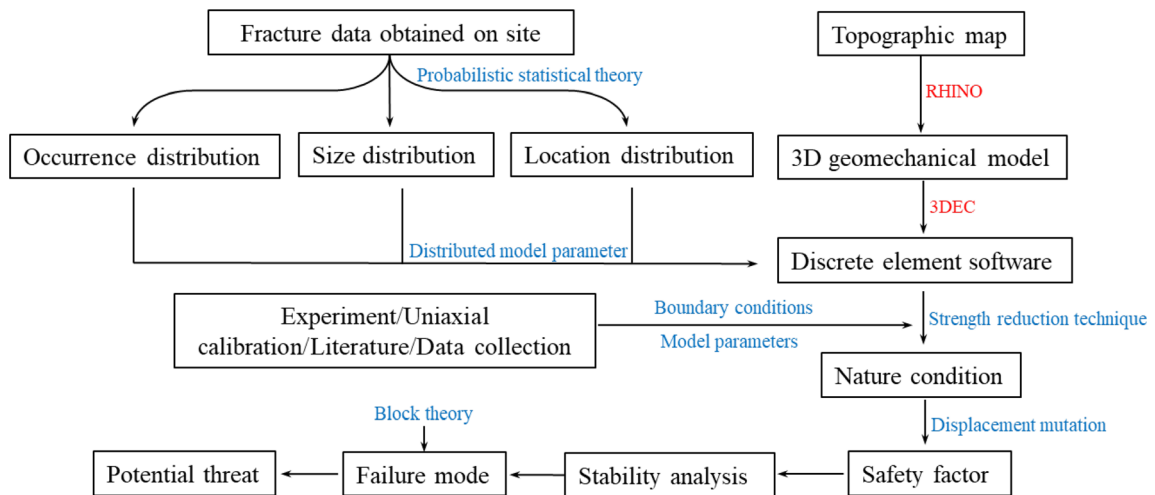


Fig. 6 Research flowchart

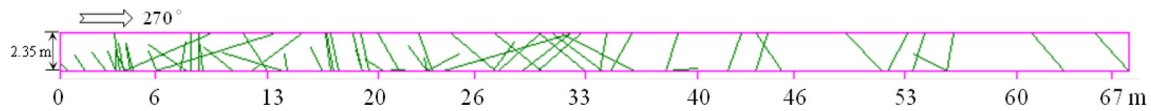


Fig. 7 Measured 2D trace length distribution map

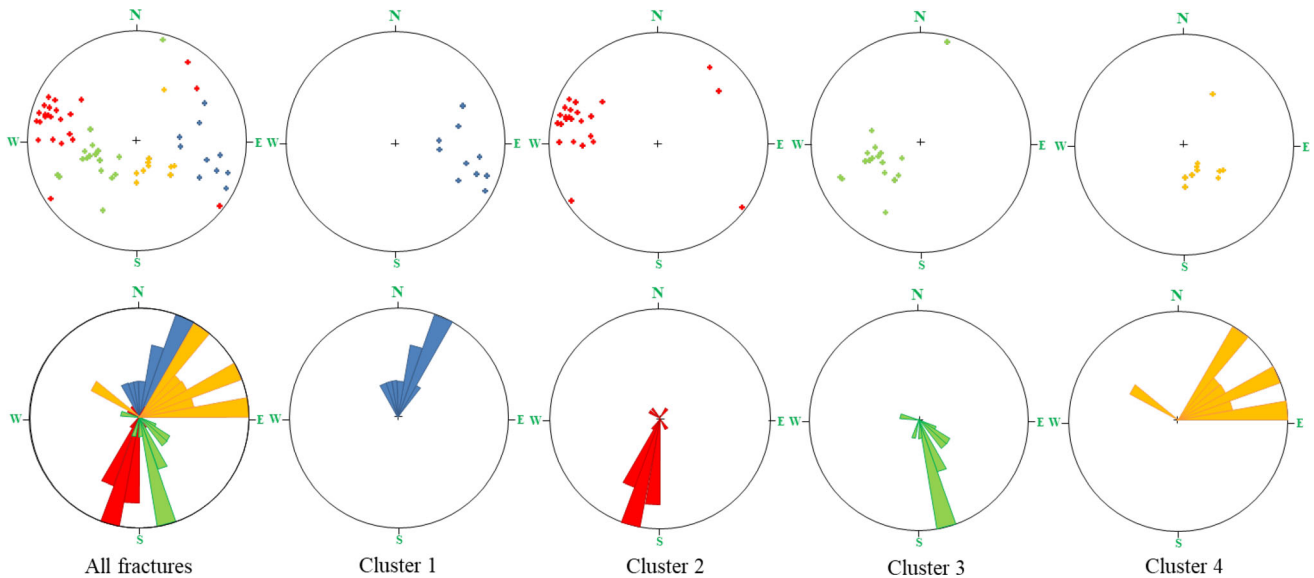


Fig. 8 The pole distribution of all fractures and each group and the corresponding strike rose map

Table 1 Correlation parameters of observed fracture data

Fracture cluster	Fracture number	Average propensity (°)	Average dip angle (°)	Fisher constant	Spherical std. (°)	Trace length			
						Measured Mean (m)	Corrected Mean (m)	Distribution type	
1	10	100.1	60.7	12.66	7.11	2.65	0.63	24.67	Log-normal
2	27	280.7	76.3	11.87	8.24	1.90	0.58	6.43	Gamma
3	17	241.2	42.0	10.35	6.44	3.06	1.02	11.88	Log-normal
4	10	145.4	26.0	35.18	2.80	4.06	2.55	14.50	Log-normal

3.2 Fracture occurrence distribution model

Fisher distribution model is used to describe the orientation of each fracture group in the study. Due to the sampling deviation regarding the orientation of discontinuities, the deviation correction is applied to the relative frequency of the measured joint orientations in order to reduce the bias [5, 43]. First, the mathematical weight of each joint in a fracture group can be calculated using Eq. (1) when fracture data are collected using a vertical sampling window:

$$W_i = \frac{\{whd_i[\cos^2\theta_i + \sin^2\theta_i\cos^2(\alpha_r - \alpha_i)]^{0.5} + 0.25\pi d_i^2[wsin\theta_i|\cos(\alpha_r - \alpha_i)|h\cos\theta_i]\}^{-1}}{\sum_{i=1}^n W_i} \quad (1)$$

where W_i is the weight formula for the i th fracture; w and h

are the width and height of the sampling window, respectively; α_i and θ_i are the dip direction and dip angle of the i th fracture, respectively; α_r is the strike of the sampling window; d_i is the fracture diameter of the i th fracture. Then, the corrected relative frequency of the i th fracture rf_i can be calculated by Eq. (2):

$$rf_i = \frac{W_i}{\sum_{i=1}^n W_i} \quad (2)$$

where n is the number of fractures in a fracture set. In the subsequent establishing of DFN, d_i is always expressed by the average fracture diameter due to the lack of the actual diameter values. In addition, the Fisher constant and the spherical standard deviation in the hemispherical

coordinate system are used to describe the discrete characteristics of each fracture group [5, 31]. The results are shown in Table 1.

3.3 Fracture size distribution model

3.3.1 Parameters of the measured trace length distribution

The maximum likelihood estimation method is used to calculate the measured trace length probability distribution for each fracture group. The equations are as follows:

$$L(\varepsilon_1, \dots, \varepsilon_i) = \prod_{j=1}^n f(l_j, \varepsilon_1, \dots, \varepsilon_i) \quad (3)$$

$$\frac{\partial L(\varepsilon_1, \dots, \varepsilon_i)}{\partial \varepsilon_i} = 0 \quad (4)$$

where ε_i is the i th parameter of the supposed probability density function; l_j is the j th trace length of the measured fracture of a fracture set. First, the probability density function $f(l_j, \varepsilon_1, \dots, \varepsilon_i)$ is assumed according to the data of the measured trace length. Then, the likelihood function $L(\varepsilon_1, \dots, \varepsilon_i)$ is obtained using Eq. (3). The parameters $\varepsilon_1, \dots, \varepsilon_i$ related to the measured trace length of the assumed probability density function are obtained by solving the likelihood function (Eq. 4). The assumed probability density function consists of five common probability distributions, such as log-normal distribution, exponential distribution, normal distribution, gamma distribution, and uniform distribution. Based on the above-mentioned process, the parameters of each assumed distribution can be obtained.

3.3.2 Kolmogorov–Smirnov Test (K–S Test)

The K–S test is a nonparametric test method that does not depend on the distribution hypothesis [17]. This method is able to effectively test the significant difference between the above-mentioned distributions of the measured trace length and the sample data. The corresponding statistic T (K–S test distance) is defined as follows [11]:

$$T = \max |F(l) - F_s(l)| \quad (5)$$

where T is the statistic of the K–S test; s is the sample size; $F(l)$ is the cumulative distribution function of the measured trace length; $F_s(l)$ is the cumulative distribution function of the sample data obtained from the assumed probability distribution (Sect. 3.3.1). The approximate significance level p , which describes the critical value T^* of the K–S test at a certain confidence level, is defined as follows [14, 23, 24]:

$$p(T \geq T^*) = 2 \sum_{i=1}^{\infty} (-1)^{i-1} e^{-2i^2 T^2 \left(\sqrt{n} + 0.12 + \frac{0.11}{\sqrt{n}} \right)^2} \quad (6)$$

The confidence level is generally set to 0.05 [14, 23, 24]. When the statistics T of a specific distribution is less than the critical value T^* at the confidence level, the distribution form of the measured trace length is acceptable. In case of multiple acceptable distributions, the best distribution is when the statistic T has the minimum value. Through the above-mentioned process, the optimal distribution form of each dominant group of the measured fractures can be determined and the corresponding average trace length and standard deviation can be obtained (Table 1).

3.3.3 Estimation of fracture size distribution

In the three-dimensional space, fractures are regarded as thin disks that are randomly distributed. Based on the stereological relationship between the true trace length distribution and the disk diameter distribution, the method proposed by Zhang and Einstein [53] can be applied to determine the disk diameter and its distribution form of each fracture group. The procedure is as follows:

1. Calculate the mean true trace length μ_l and the standard deviation σ_l ($\sigma_l = \mu_l (COV)_m$) of the true trace length distribution [22], where $(COV)_m$ is the coefficient of variation of the measured trace length distribution;
2. Estimate the distribution of disk diameter from the true trace length distribution. First, it is assumed that a fractured disk obeys a certain probability distribution. Then, the mean diameter μ_D and the standard deviation σ_D of the fracture size distribution are calculated based on the Warburton equation [43, 53]. The equations are as follows:

$$\mu_l = \frac{\pi \left[(\mu_D)^2 + (\sigma_D)^2 \right]}{4\mu_D} \quad (7)$$

$$\left[(\mu_l)^2 + (\sigma_l)^2 \right] = \frac{2E(D^3)}{3\mu_D}$$

where $E(D^m)$ is the m th moment of the fracture diameter, $m = 1, 2, 3, \dots$. It is necessary to test the assumed type of the fracture disk diameter distribution using following equation:

$$\frac{E(D^4)}{E(D^2)} = \frac{4E(l^3)}{3E(l)} \quad (8)$$

where $E(l^m)$ is the m th moment of the trace length, $m = 1, 2, 3, \dots$. The closer the two sides of Eq. (8) are, the better the type of distribution. Based on the measured trace length distribution, two common distributions (log-normal and gamma distribution) are selected as the assumed distribution of true trace length. Based on the above-mentioned

process for estimating the disk diameter distribution, the optimal diameter distribution of each fracture group can be obtained (Table 2).

3.4 Fracture location distribution model

3D fracture spacing can be obtained from 2D fracture spacing. The 2D fracture spacing can be calculated on the basis of fracture data from the field according to the method from Karzulovic and Goodman [18]. When the fracture shape is considered a disk and the center of the disk obeys the homogeneous Poisson distribution, the spatial density ρ_i^V (V : volume of simulated space region) in unit volume of each fracture group is determined by the corresponding normal line density ρ_i^N in Eq. (9) [21, 33]. After the calculation, the volume densities of the spatial distribution of four fracture groups are 0.001, 0.018, 0.005, and 0.004, respectively.

$$\rho_i^V = \frac{4\rho_i^N}{\pi E(D^2)}. \tag{9}$$

3.5 3D DFN and model test

In accordance with the needs of engineering simulation, the size of the 3D DFN should be 270 m × 240 m × 240 m. This size can fully cover the proposed tunnel entrance and various bridge projects and meets the design requirements. However, in order to eliminate the boundary effect, the fracture simulation space is set at 300 m × 270 m × 270 m [14]. In combination with the volume density of the fracture distribution, the number of fractures in each fracture group can be determined. The Monte Carlo simulation is used to generate DFN that includes the distribution model of the occurrence, size, and location of fractures. To reduce the error caused by the contingency of model generation, each model is randomly generated five times [14, 55] and 125 DFNs are obtained. To verify the validity

of the generated model, a window with the same specifications and parallel to the field sampling window is placed in the DFN to cut the simulated rock mass and obtain the simulated fracture information. By comparing the 2D trace length diagram of the generated model and the on-site sampling window, the number of exposed fractures, mean occurrence, mean observed trace length, mean corrected trace length and exposure ratios of different fracture types, and an optimal generated model can be obtained. The 2D trace length comparison of the optimal DFN model and the measured data is shown in Fig. 9, and the comparison among the corresponding statistical parameters is shown in Table 3. The simulation results are acceptable.

3.6 Discrete element method

DEM was developed in 1979 [8] as a method to more realistically express geometric characteristics and to analyze nonlinear deformations of jointed rock masses. Thus, it is commonly used to simulate slope stability. The basic principle of DEM is based on Newton’s second law. It is assumed that rock blocks cut by fractures have rigid or deformable characteristics. These rock blocks are arranged in a mosaic and form a rock mass, with each rock block in equilibrium. If there is a change in external force or displacement boundary, the rock block and adjacent blocks will be displaced until the rock mass is broken. Therefore, DEM can explain rock mass deformation and is suitable for numerical stability analysis. The SRM is commonly used in slope stability analysis [1, 4, 45]. Since the joints control the strength of the rock mass, the strength parameters of the rock mass and joints should be simultaneously reduced when SRM is used. The shear strength is reduced by introducing the strength reduction factor (SRF) as follows:

$$\begin{aligned} C' &= \frac{C}{SRF} \\ \phi' &= \arctan\left(\frac{\tan\phi}{SRF}\right) \end{aligned} \tag{10}$$

Table 2 Determination of the diameter distribution of the fractured disk

Fracture group	Assumed distribution form of $g(D)$	μ_l	σ_l	$E(D)^4/E(D)^2$	$4E(l^3)/3E(l)$	Optimal distribution form of $g(D)$
1	Log-normal	2.5	0.4	14.43	8.99	Log-normal
	Gamma	3.4	0.6	24.41		
2	Log-normal	0.9	0.7	4.30	1.89	Gamma
	Gamma	1.5	0.5	2.33		
3	Log-normal	3.4	1.2	21.11	21.92	Log-normal
	Gamma	4.1	0.7	36.37		
4	Log-normal	4.3	1.9	40.54	42.10	Log-normal
	Gamma	4.7	2.2	60.62		

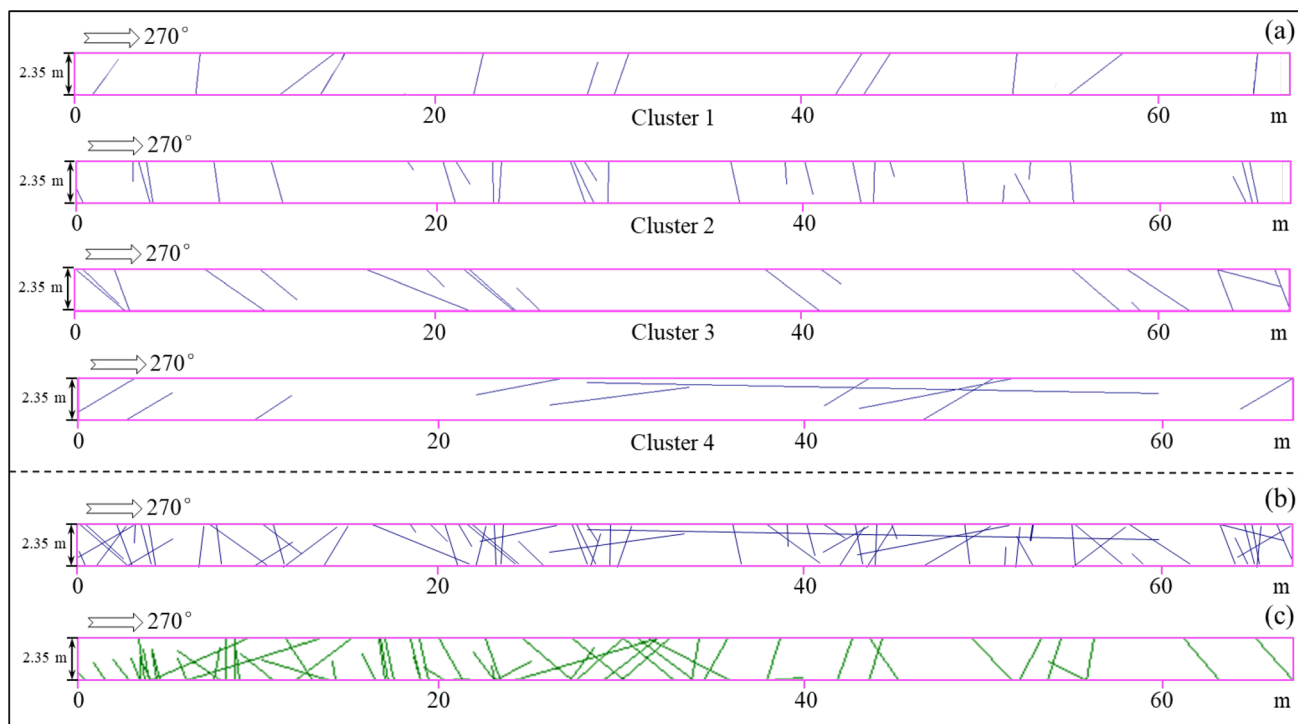


Fig. 9 Comparisons between measured and simulated trace length maps: **a** four groups of simulated trace length maps, **b** simulated trace length map, and **c** measured trace length map

Table 3 Comparison of statistical parameters between the generated model and field data

Fracture set	Field or generated	Mean dip direction	Mean dip angle	Measured trace length	Corrected trace length	Ratio of R ₀ , R ₁ , and R ₂	Fracture number
1	Field	100.1°	60.7°	2.65 m	24.67 m	0.80/0.20/0	10
	Generated	101.0°	59.1°	2.53 m	24.51 m	0.83/0.17/0	12
2	Field	280.7°	76.3°	1.90 m	6.43 m	0.44/0.56/0	27
	Generated	283.5°	77.5°	2.00 m	6.94 m	0.48/0.52/0	29
3	Field	241.2°	42.0°	3.06 m	11.88 m	0.53/0.47/0	17
	Generated	245.5°	45.3°	2.85 m	11.18 m	0.53/0.47/0	18
4	Field	145.4°	26.0°	4.06 m	14.50 m	0.5/0.3/0.2	10
	Generated	142.1°	29.9°	4.60 m	14.50 m	0.5/0.4/0.1	10

R₀: Fractures not exposed at both ends; R₁: Fractures exposed at one end; and R₂: Fractures exposed at both ends

where C is the initial cohesion; φ is the initial internal friction angle; C' and φ' are reduced cohesion and internal friction angle, respectively. The criterion of model failure is an important condition for measuring the completion of calculation. In the finite element model, four main failure criteria can be applied to assess the slope failure based on the strength reduction method [1], i.e., numerical non-convergence, excessive equivalent plastic strain, plastic zone connection, and displacement mutation. Although stability analysis based on discrete element model can refer to these criteria, they are not completely applicable. First,

the non-convergence criterion in DEM cannot provide the cause and mode of failure, and even when the overall slope stability is good and there is a local failure, the model will still be judged as failure. This can lead to misjudgment of the slope stability. Second, the discrete element uses joint sliding or block detachment as a local failure criterion instead of entering the plastic stage. Therefore, the first three failure criteria are not very suitable for the stability analysis of rocky slopes, and the displacement mutation criterion is adopted in this study.

Before the stability analysis, it is important to determine the constitutive model and strength parameters of the

material. In this study, the Mohr–Coulomb criterion is selected as the constitutive model of rock blocks and fractures. Rock parameters, such as density and uniaxial compressive strength are obtained by laboratory experiments on standard rock samples. The on-site rebound test is used to verify the results of the uniaxial compressive strength test. Other parameters of rock blocks and fractures are calibrated using the uniaxial compression experimental model of standard rock samples. First, a rock block with a side length of 1 m is established. Four groups of joints with Fisher distribution are defined on the basis of the actual dominant occurrence of fractures in the rock mass. The joint size distribution type is set to be the same as the fracture diameter distribution determined in Sect. 3.3. The minimum and maximum joint diameters are set at 0.1 m and 1 m, respectively. The fracture location is set as the random uniform distribution. Then, the bottom of the model is fixed and the vertical downward velocity (v_p) is applied to the upper boundary in order to simulate loading. The rock and fracture strength parameters (the strength parameters of the virtual fracture are consistent with the rock) are adjusted until the calculated uniaxial compressive strength is basically consistent with the test value. The final results of the model calibration are shown in Fig. 10, while the rock and fracture strength parameters are shown in Table 4.

4 Modeling

The coordinates of the center, the diameter, and the occurrence of each disk in the previously generated optimal DFN are imported into the 3DEC software in the form of a text file. A DFN containing 6.06×10^5 fractures can

Table 4 Calculation parameters of blocks and joints

Type of parameters	Compression test parameters
Block density (kg/m^3)	2600
Block elastic modulus E (GPa)	14.10
Poisson’s ratio ν	0.26
Block shear modulus G (GPa)	5.595
Block bulk modulus K (GPa)	9.79
Block tensile strength (MPa)	4
Block cohesion (MPa)	9
Friction angle ($^\circ$)	35
Joint normal stiffness (GPa/m)	9
Joint shear stiffness (GPa/m)	3
Joint tensile strength (MPa)	0.21
Joint cohesion (MPa)	0.2
Joint friction angle ($^\circ$)	30

effectively reflect the distribution of fractures in the actual rock slope (Fig. 11). It can be noticed that most of the fractures are tiny cracks. However, DFN with a large number of fractures is difficult to use directly in the model calculation. Moreover, majority of the unconnected micro fractures in the DFN have little influence on the mechanical rock parameters. Therefore, it is necessary to adopt an efficient and simplified DFN in order to reduce the number of fractures.

To determine the simplified DFN standard, the uniaxial compression test model of the fractured rock mass is used to analyze the influence of fracture size and number on the rock strength. The specific steps are as follows:

1. A cube block with a side length of 1 m has been established because excessive block size with too many joints in the DFN would increase the calculation time. On

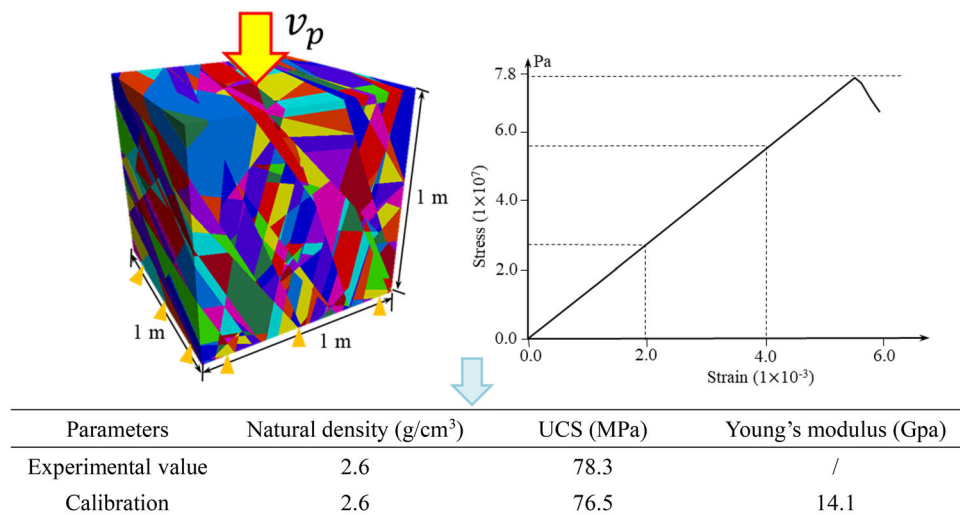


Fig. 10 Parameter calibration model for uniaxial compression experiments

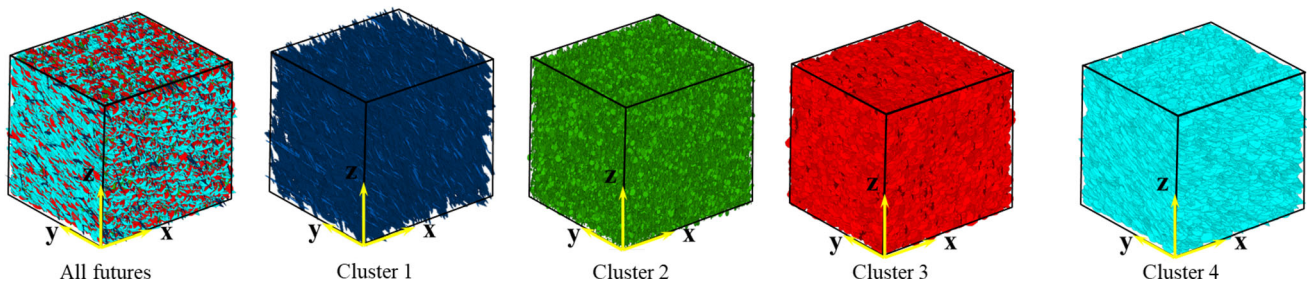


Fig. 11 Simulated 3D DFN

the other hand, dense and short joints create tiny blocks that can interrupt the calculation. Furthermore, the size of the block would be too small to characterize the DFN well. Therefore, it is appropriate to set the side length of the cube to 1 m [50]. Four groups of dominant joints are generated with the same occurrence as the field data and satisfying the Fisher distribution. The joint size distribution type is consistent with the field data, and the minimum and maximum disk diameters are set to 0.1 m and 1 m, respectively. The joint positions are set as uniform distribution;

2. Using the built-in Fish language programming of the 3DEC software, disks with a diameter less than or equal to 0.1 m, 0.2 m, 0.3 m, 0.4 m, 0.5 m, 0.6 m, 0.7 m, 0.8 m, 0.9 m, and 1 m are removed and corresponding simplified fracture networks are obtained (Fig. 12a, b); and

3. The fractured rock mass model was obtained by cutting rock blocks with different fracture networks (Fig. 12c, d). The Mohr–Coulomb criterion was selected as the constitutive model. Strength parameters were determined by the compression experimental model (Table 4). The bottom of the model is fixed, while the upper boundary moves vertically downward at a constant speed (v_p) of 0.05 m/s. During the calculation, stress–strain curves are recorded (Fig. 13a) and the compressive strength of different models is analyzed (Fig. 13b).

Deleting the fractures with a diameter of 0.1 ~ 0.4 m has little effect on the strength of the rock mass model. However, after the fractures with a diameter greater than 0.4 m are deleted, the strength of the rock mass increases significantly. This change becomes more obvious as the diameter of the deleted fracture increases. Therefore, it can be considered that a fracture with diameter smaller than the first 40% of the size distribution has little influence on the rock strength. However, different rock block shapes and sizes may lead to changes in the law of rock and soil strength [7, 26]. In order to further explore this law, we set up compression tests with side lengths of 5 m (fracture size range 0.5–5 m), 10 m (fracture size range 1–10 m), and 15 m (fracture size range 5–15 m). The parameters of

fracture distribution (occurrence, size, and position distribution) are the same as those of standard cube compression test except for the fracture size range. The results (Fig. 13c, d, and e) show that for the experimental groups of different sizes, although the compressive strength has changed, there is a turning area of strength. This area is generally distributed in the first 30%–40% of the fracture size range. Once the size of the removed fracture exceeds the first 40% of the size range, the rock mass strength increases significantly. That is to say, when the fracture distribution characteristics in the study area are constant, the influence of small fractures in the first 30–40% of the fracture size range on the strength of rock mass is small. This rule is similar to the result of cube compression experiment with side length of 1 m. Considering the limitation of computer performance, this law can be extended to study the right bank rocky slope of Yigong Zangbu Bridge to greatly simplify the fracture network, which is of great significance to apply the DFN (obtained from measured data) to engineering practice.

According to the above-mentioned rules, the previously generated DFN model of rock slope can be simplified. Since the maximum fracture diameter in DFN is 101 m, the impact of fractures with a diameter less than 40 m (first 40%) is not considered, and only large fractures are considered for the calculation. The simplified DFN is shown in Figure 14a. Then, a 3D model of the rock slopes on the right bank of Yigong Zangbu Bridge was set up based on the DEM (Fig. 14b). The 3D modeling software Rhino [2] can realize the process and import the model into 3DEC directly. Finally, taking the adit position as a reference, the 3D geomechanical model of the fractured rock slope was obtained by cutting the rock slope with DFN (Fig. 14c).

The initial conditions of the model should take into account the characteristics of high geo-stress in the study area. Guo [13] proposed a modified equation for calculating geo-stress in southeastern Tibet using measured stress values obtained from several typical hydropower stations and 12 geo-stress measurement stations. The equation puts

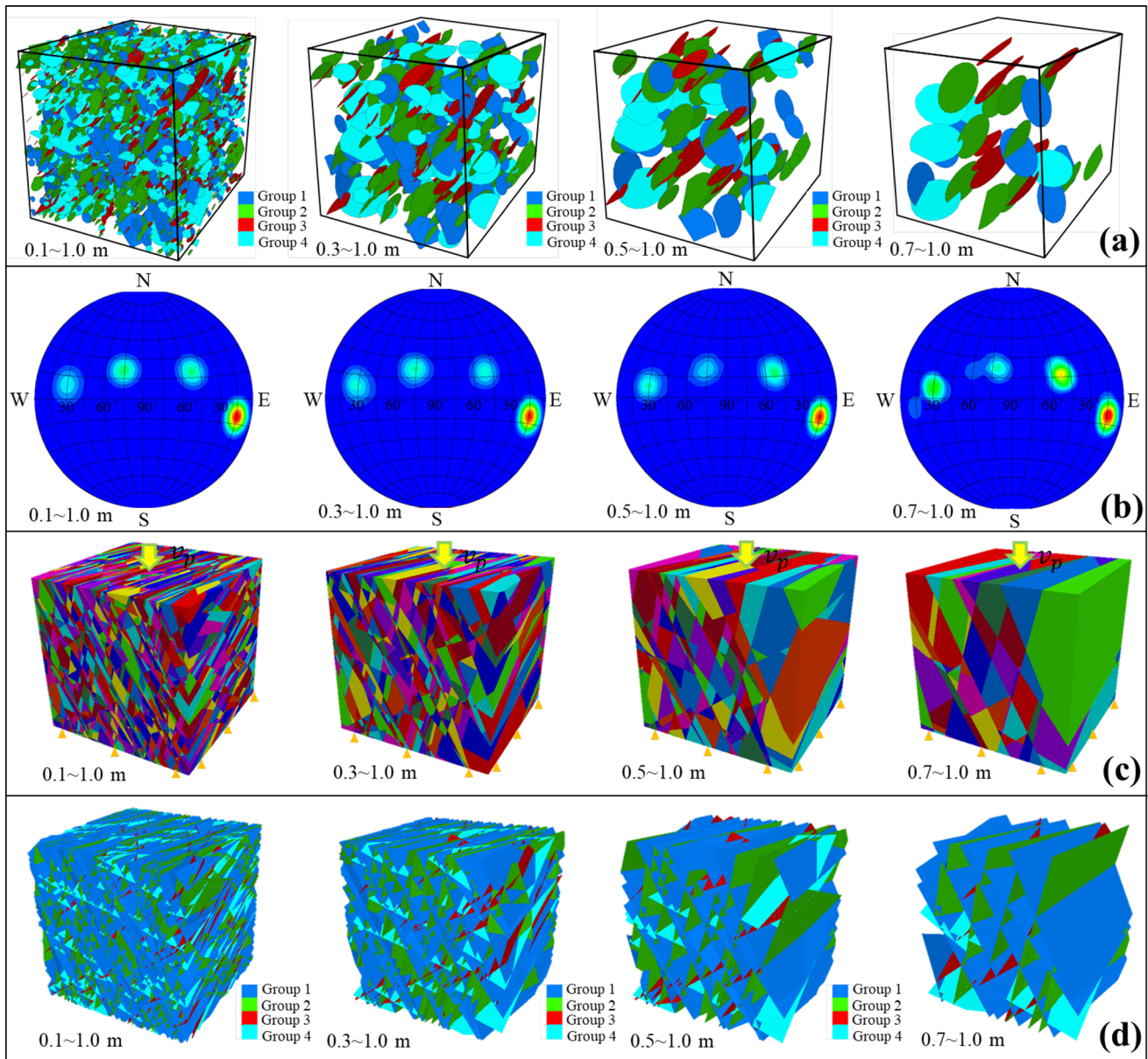


Fig. 12 Uniaxial compression test model with removed joints of different sizes: **a** DFN, **b** Schmidt projection of joints, **c** block model, and **d** joint model

forward a new concept named relative focal depth based on the traditional empirical equation and considers that the high geo-stress area generally has a considerable crust thickness and frequent earthquakes. The thickness of the crust is directly related to the uplift rate. The introduction of historical focal depth and corresponding crustal thickness reduced the error in calculating geo-stress in different regions by traditional empirical equation. In Guo’s equation [13], the maximum horizontal principal stress is obtained as follows:

$$\sigma_H = 15.48 - 29.62x + 0.0261H (R^2 = 0.8) \tag{11}$$

where σ_H is the maximum horizontal crustal-stress; x is the relative focal depth of the study area; H is the evaluation depth; R^2 is the goodness of fit of the equation. The average focal depth of the historical earthquake in the study area is from 22 to 25 km. The average crustal thickness is 65 km, and the maximum principal stress is 46.3°NE . The minimum horizontal crustal-stress σ_h and vertical stress σ_V are then determined by Eq. (12) as follows:

$$\begin{aligned} \sigma_h &= \sigma_H - 0.0058H - 2.912 \\ \sigma_V &= 0.0271H. \end{aligned} \tag{12}$$

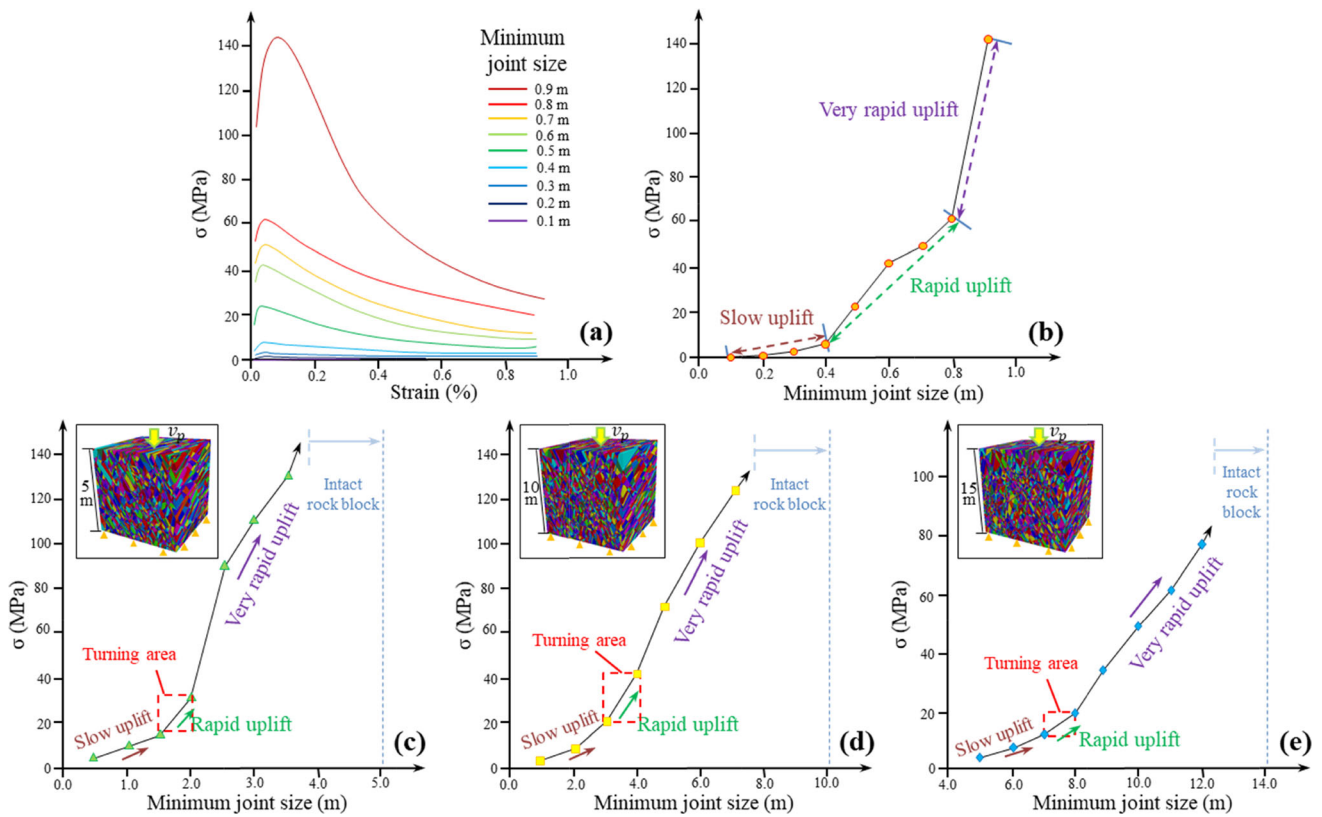


Fig. 13 **a** Stress–strain curves of uniaxial compression test model (side length of 1 m) with removed joints of different sizes, **b** change in strength of uniaxial compression test model (side length of 1 m) with removed joints of different sizes, **c** change in compressive strength of a cube with side length of 5 m after removing joints of different sizes, **d** change in compressive strength of a cube with side length of 10 m after removing joints of different sizes, and **e** change in compressive strength of a cube with side length of 15 m after removing joints of different sizes



Fig. 14 **a** Simplified DFN model of the rock slope, **b** 3D model of the right bank, and **c** 3D geomechanical model of the right bank

Since the real stress direction does not coincide with the coordinate axis of the model, it is necessary to rotate the coordinate to resolve the initial geo-stress, which is then applied to the model. The six initial stress states after the transformation are given in Eq. (13):

$$\begin{aligned}
 \sigma_x &= 3.13 + 0.023H \\
 \sigma_y &= 1.1851 + 0.0224H \\
 \sigma_z &= 0.0271 \\
 \tau_{xy} &= 1.453 + 0.007H \\
 \tau_{yz} &= 0 \\
 \tau_{zx} &= 0.
 \end{aligned}
 \tag{13}$$

The boundary conditions of the model are as follows: the normal displacement is limited to 0 for the four lateral sides of the model; the displacement in three directions is 0 for the bottom boundary; and the upper boundary of the model is free. SRM is used to analyze the stability of rock slopes, while different reduction factors (1 ~ 2.4) are used to reduce the shear strength of the material. By monitoring the deformations of some rock blocks, the displacement mutation criterion is used to assess the slope stability. When the displacement of the monitored rock mass

changes abruptly, the slope is regarded as failure and the strength reduction factor is the slope safety factor.

5 Results

Four monitoring points are placed at different positions of the slope to monitor the displacement. The range of strength reduction factor is from 1.0 to 2.4 and the increment of each calculation is set to 0.1. Figure 15 shows the slope displacement diagram under different strength reduction factors. The results show that the overall slope stability is good. Furthermore, the deformation trend with different reduction factors is similar, but the deformation increases with increasing reduction coefficient. The deformation is mainly concentrated at the toe of the slope, and the maximum displacement can reach 2.35×10^{-1} m. It can be noticed that when SRF is greater than 2.0, the slope displacement increment is basically 0. Nevertheless, obvious tensile fractures appear in the lower part of the slope and some rock masses fall off at that point. To determine the slope safety factor, the z-displacement and x-displacement curves of four monitoring points are recorded in Fig. 16. It can be found that when SRF is 2.0, displacement increment of each monitoring point shows abrupt changes. According to the displacement mutation criterion, the safety factor of the rock slope on the right bank of Yigong Zangbu Bridge is 2.0. Therefore, it can be considered that the slope is stable in its natural state, yet there is a possibility of the local block falling into the lower part of the slope.

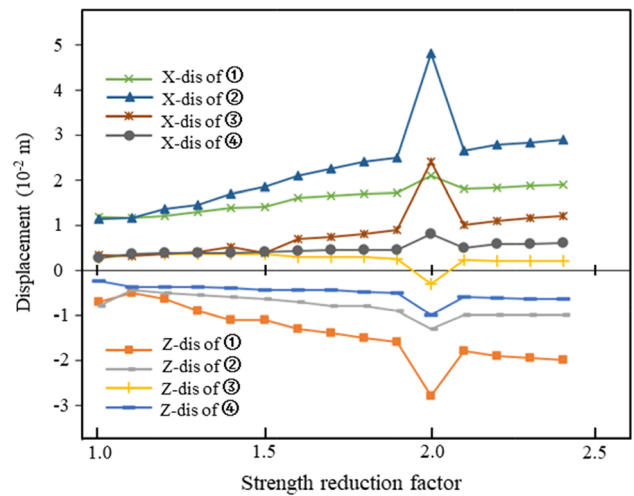


Fig. 16 Variation of x-direction and z-direction displacement of different monitoring points with strength reduction coefficient

The simulation results are consistent with the field investigation. Obvious collapse of blocks was noticed at the lower part of the slope (Fig. 17a), thus damaging the road and the guardrail by falling stones (Fig. 17b). At the foot of the slope are noticed tension fractures in the deformed rock mass (Fig. 17c). These field observations confirm the simulation results well.

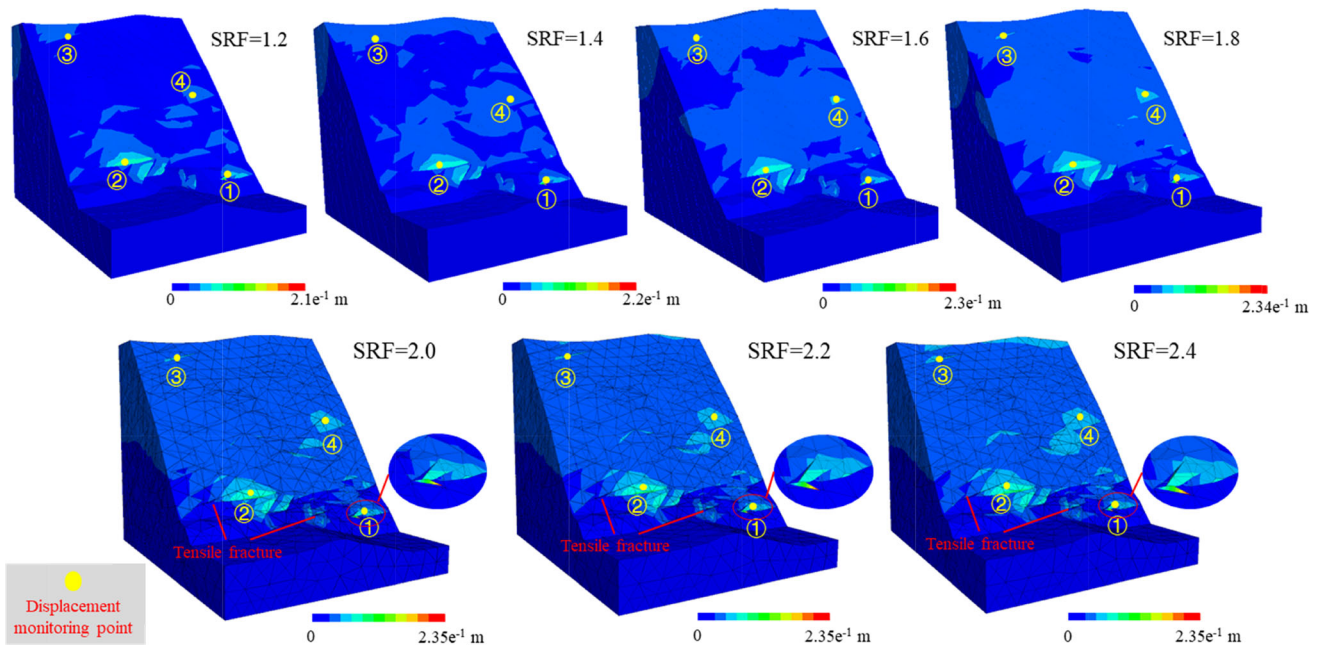


Fig. 15 Displacement maps of the rock slope under different SRF

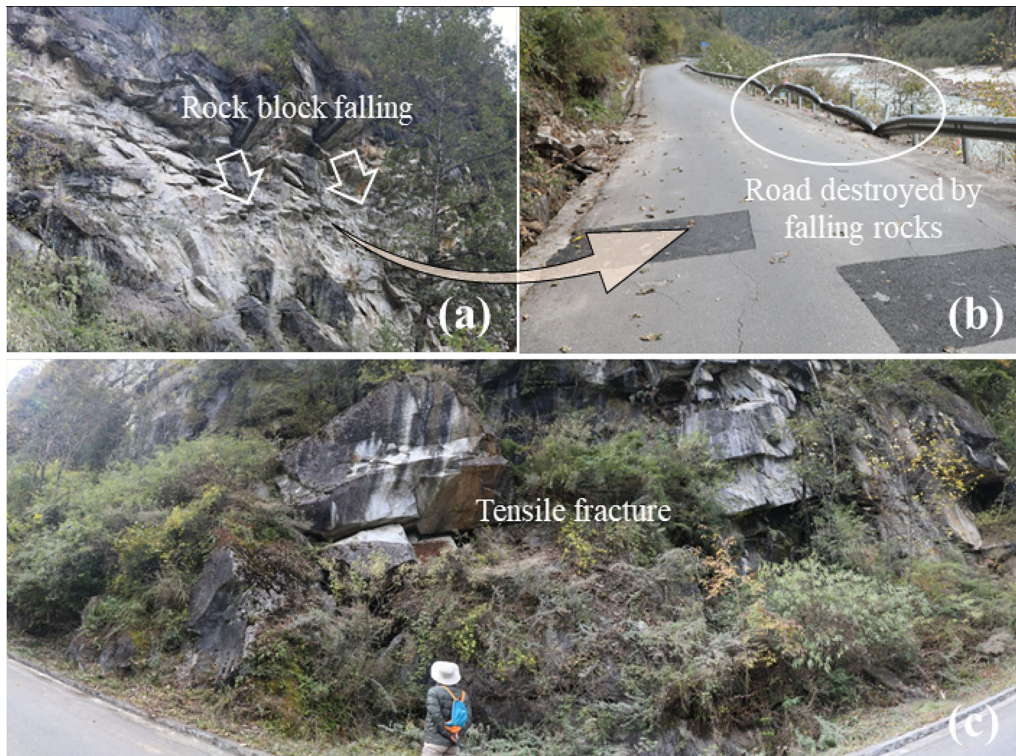


Fig. 17 **a** Rock falling phenomenon, **b** road destroyed by falling rocks, and **c** tension fractures developed in the rock slope

6 Discussion

The results of the numerical simulation reflect that the joints and fractures control the deformation of the rock slope. The cutting relationship of the four groups of dominant fractures in DFN has a key role. To further analyze the deformation mechanism, the dynamic analysis method based on the block theory is applied to discuss the failure mode of the rock slope. This method can extend the planar stereographic projection (used to express the occurrence of structural planes in engineering geological problems) to full-space stereographic projection [38–40]. The full-space stereographic projection enables some concepts and theorems of block theory in 3D space to be represented by corresponding 2D projection areas [20, 30]. Therefore, it has strong operability.

With the help of full-space stereographic projection based on the geometric mobility judgment theorem in the block theory, the cutting relationship between the empty face and the spatial structure surface is studied in order to analyze the mechanism of collapse formation. First, four groups of dominant fractures in the rock slope were combined with free surfaces for the stereographic projection (Fig. 18a). For the right bank, the structural plane J_3 intersects with the free surface at a large angle, which mainly serves as a lateral separation. J_2 inclines inside the slope at a steep angle and plays the role of vertical

separation and easily forms the unloading fractures. The structural planes J_1 and J_4 are gently inclined out of the slope. After cutting and combining with the other two groups of structural planes, movable blocks are easily formed, which is unfavorable to the stability. However, the dominant structural planes cannot represent all discontinuities, and some important structural planes may be ignored. To solve this problem, an additional investigation of the fractures on the rock slope surface is performed and some representative structural planes are selected for the full-space stereographic projection (Fig. 18b). The results show that the steeply inclined structural planes RJ_1 and RJ_3 , which are intersecting the free surface of the slope at a large angle, form the lateral separation plane of the rock block. The second structural plane RJ_2 , which is steeply inclined outside the slope and whose dip angle is greater than the slope angle, becomes the vertical separation plane. However, due to the existence of a structural plane RJ_4 that is slightly inclined outside the slope (i.e., the dip angle is less than the slope angle), the combined cutting of the four groups of fractures is likely to create unfavorable blocks with RJ_4 as the slip surface, so the local collapse may occur.

The block theory fundamentally explains the macroscopic performance and the results of the stability analysis of the rock slope. For the right bank of Yigong Zangbu

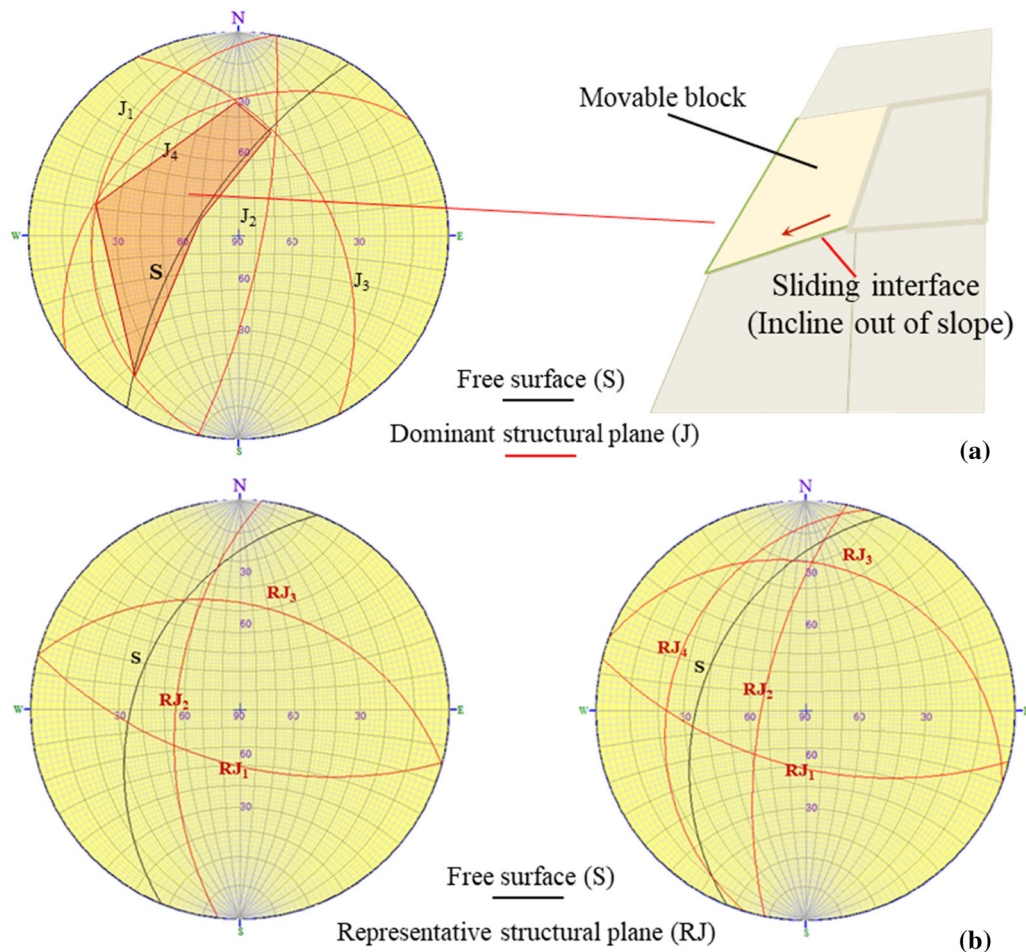


Fig. 18 Stereographic projections of the dominant structural planes and the air-facing surfaces on the right bank of Yigong Zangbu Bridge, as well as the conceptual model of the structural block

Bridge, it is likely to form unstable and falling blocks, which is in line with the field investigation.

In this paper, DFN and DEM combined with SRM are used to analyze the slope stability of massive rocks. The results are reasonable and valuable for engineering design and disaster prevention. Nevertheless, there are certain shortcomings, such as the simplified standard of DFN and the proper application of SRM. The DFN obtained from the fracture data that is acquired from the field investigation and based on the probability and statistics theory has better applicability in the small-scale model [14]. In the analysis of large-scale model, due to limited performance of model and software, it is necessary to simplify the DFN, which to some extent changes the distribution characteristics of local fractures. In addition, the applicability of SRM in continuous media is better. Although DEM software combines this method with general DEM blocks and the strength parameters of deformable blocks and joints of rock slopes with multiple structural planes are reduced for stability analysis, the failure mechanism of massive rock mass

differs from that of a continuous medium. Therefore, it is necessary to establish an equivalent model of the rock mass structure in order to achieve the transition from the non-continuum to continuum media, which is the focus of future work.

7 Conclusion

Yigong Zangbu Bridge is an essential part of the Sichuan–Tibet Railway. Therefore, it is important to determine the stability of the rock slopes on both sides for the external safety assessment of the bridge. In order to reflect the development characteristics of joints and fractures on the rock slope, the method based on probability and statistics theory is used to determine the occurrence, size, and location distribution model according to the fracture data obtained from the field. DFN is then developed in the 3DEC discrete element software and used to cut 3D model of the rock slope. The distribution characteristics of the

fractures in the rock slope are largely reflected. The results of the stability calculation show that the overall stability of the right bank is good. However, local damage may occur. The distribution of joints and fractures controls the deformation of the rock slope, and the cutting relationship of the four groups of dominant fractures in the DFN has a decisive role. The failure mode is mostly characterized by the local block collapse, which concentrates in the lower part of the slope. In combination with dynamic analysis based on the block theory, the dominant structural planes and free surfaces that are developed on the right bank can form rock blocks of different sizes by combining and cutting each other. Due to the existence of structural planes that gently inclined out of the slope, movable blocks are easily formed and destroyed under the action of geological forces. Therefore, more attention should be paid to the threat of a local block falling in the lower part of the rock slope, which is also the main threat to the bridge. This study established a complete evaluation of the slope stability, including field investigation, indoor interpretation, DFN generation, 3D fractured rock slope establishment, and stability analysis. The influence of the distribution characteristics of fissures on slope stability is fully considered. The results are significant for engineering design and disaster prevention.

Acknowledgements This work was supported by the National Natural Science Foundation of China (Grant Nos. 41941017, U1702241) and the National Key Research and Development Plan (Grant No. 2018YFC1505301). The authors would like to thank the editor and anonymous reviewers for their comments and suggestions which helped a lot in making this paper better.

References

- Bao YD, Han XD, Chen JP, Zhan JW, Zhang W, Sun XH, Chen MH (2019) Numerical assessment of failure potential of a large mine waste dump in Panzhihua City, China. *Eng Geol* 253:171–183
- Bao YD, Zhai SJ, Chen JP, Xu PH, Sun XH, Zhan JW, Zhang W, Zhou X (2020) The evolution of the Samaoding paleo-landslide river blocking event at the upstream reaches of the Jinsha River Tibetan Plateau. *Geomorphology* 351:106970
- Camones LAM, Vargas EDA, De Figueiredo RP, Velloso RQ (2013) Application of the discrete element method for modeling of rock crack propagation and coalescence in the step-path failure mechanism. *Eng Geol* 153:80–94
- Chen JF, Liu JX, Xue JF, Shi ZM (2014) Stability analyses of a reinforced soil wall on soft soils using strength reduction method. *Eng Geol* 177:83–92
- Chen JP, Xiao SF, Wang Q (1995) Three-dimensional network modeling of stochastic fractures. Northeast Normal University Press, Changchun
- Chuan-Bin W, Shi B, Sun Y, Zhao YG (2004) Numerical simulation analyses on stability of the No.3 tunnel of Bainijing in Kunming by FLAC-3D. *Hydrogeol Eng Geol* 31(6):52–55
- Cui SW, Tan Y, Lu Y (2020) Algorithm for generation of 3D polyhedrons for simulation of rock particles by DEM and its application to tunneling in boulder-soil matrix. *Tunn Undergr Space Technol* 106:103588
- Cundall P, Strack O (1979) A discrete numerical model for granular assemblies. *Geotechnique* 29:47–65
- Dershowitz WS, La Pointe PR, Doe TW (2004) Advances in discrete fracture network modeling. In: Proceedings of the US EPA/ NGWA fractured rock conference, Portland, ME, 882–894
- Dowd PA, Xu C, Mardia KV, Fowell RJ (2007) A comparison of methods for the stochastic simulation of rock fractures. *Math Geol* 39:697–714
- Drew JH, Glen AG, Leemis LM (2000) Computing the cumulative distribution function of the Kolmogorov-Smirnov statistic. *Comput Stat Data An* 34:1–15
- Farah K, Ltfi M, Hassis H (2011) Reliability analysis of slope stability using stochastic finite element method. *Procedia Eng* 10:1402–1407
- Guo Y (2015) Research on Evaluation Method of In-situ Stress in Southeastern Margin of Qinghai-Tibet Plateau. Master's thesis, Southwest Jiaotong University, Sichuan
- Han XD, Chen JP, Wang Q, Li YY, Zhang W, Yu TW (2016) A 3D fracture network model for the undisturbed rock mass at the Songta dam site based on small samples. *Rock Mech Rock Eng* 49:611–619
- Hatzor YH, Arzi AA, Zaslavsky Y, Shapira A (2004) Dynamic stability analysis of jointed rock slopes using the DDA method: King Herod's Palace, Masada, Israel. *Int J Rock Mech Min Sci* 41(5):813–832
- Ivanova VM, Sousa R, Murrhoy B, Einstein HH (2014) Mathematical algorithm development and parametric studies with the GEOFRAC three-dimensional stochastic model of natural rock fracture systems. *Comput Geosci* 67:100–109
- Johnson RA, Bhattacharyya GK (2009) Statistics: principles and methods, 6th edn. Wiley, Hoboken
- Karzulovic A, Goodman RE (1985) Determination of principal joint frequencies. *Int J Rock Mech Min Sci Geomech Abstr* 22:471–473
- Kemeny J, Post R (2003) Estimating three-dimensional rock discontinuity orientation from digital images of fracture traces. *Comput Geosci* 29:65–77
- Kocharyan GG, Brigadin IV, Karyakin AG, Kulyukin AM, Ivanov EA (1995) Study of caving features for underground workings in a rock mass of block structure with dynamic action. Part IV. effect of rock mass structure on the stability of mine workings. *J Min Sci* 31:1–7
- Kulatilake PHSW, Wathugala DN, Stephansson OVE (1993) Stochastic three-dimensional joint size, intensity and system modelling and a validation to an area in Stripa Mine, Sweden. *Soils Found* 33:55–70
- Kulatilake PHSW, Wu TH (1984) Estimation of mean trace length of discontinuities. *Rock Mech Rock Eng* 17:215–232
- Li XJ, Zuo YL, Zhuang XY, Zhu HH (2014) Estimation of fracture trace length distributions using probability weighted moments and L-moments. *Eng Geol* 168:69–85
- Li YY, Wang Q, Chen JP, Han LL, Song SY (2014) Identification of structural domain boundaries at the Songta dam site based on nonparametric tests. *Int J Rock Mech Min Sci* 70:177–184
- Lu Y, Tan Y, Li X (2018) Stability analyses on slopes of clay-rock mixtures using discrete element method. *Eng Geol* 244:116–124
- Lu Y, Tan Y, Li X, Liu C (2017) Methodology for simulation of irregularly shaped gravel grains and its application to DEM modeling. *J Comput Civ Eng* 31(5):04017023
- Lv Q, Liu Y, Yang Q (2017) Stability analysis of earthquake-induced rock slope based on back analysis of shear strength parameters of rock mass. *Eng Geol* 228:39–49

28. Marcotte D, Henry E (2002) Automatic joint set clustering using a mixture of bivariate normal distributions. *Int J Rock Mech Min Sci* 39:323–334
29. Mauldon M, Dunne WM, Rohrbaugh MB (2001) Circular scanlines and circular windows: new tools for characterizing the geometry of fracture traces. *J Struct Geol* 23:247–258
30. Meng QB, Han LJ, Xiao Y, Li H, Wen SY, Zhang J (2016) Numerical simulation study of the failure evolution process and failure mode of surrounding rock in deep soft rock roadways. *Int J Min Sci Techno* 26(2):209–221
31. Min KB, Jing L, Stephansson O (2004) Determining the equivalent permeability tensor for fractured rock masses using a stochastic REV approach: method and application to the field data from Sellafield, UK. *Hydrogeol J* 12:497–510
32. Munier R (2004) Statistical analysis of fracture data, adapted for modelling discrete fracture networks—version 2. Swedish Nuclear Fuel and Waste Management Company, Stockholm
33. Oda M (1982) Fabric tensor for discontinuous geological materials. *Soils Found* 22:96–108
34. Osada M, Shrestha SK, Kajiyama T (2005) Application of rock mass integration method (RMIM) with DDA modeling in rock slope stability. *Contrib Rock Mech New Century* 1–2:1257–1262
35. Regassa B, Xu N, Mei G (2018) An equivalent discontinuous modeling method of jointed rock masses for DEM simulation of mining-induced rock movements. *Int J Rock Mech Mining Sci* 108:1–14
36. Riley MS (2005) Fracture trace length and number distributions from fracture mapping. *J Geophys Res-Sol Ea* 110(B8):B08414
37. Seismic parameter zoning map of China (GB18306–2015) (2015) Published by the National Standardization Management Committee of China
38. Shi GH (1977) Stereoscopic projection method for rock stability analysis. *Chin Sci* 3:269–271 ((In Chinese))
39. Shi GH, Goodman RE (1988) Block Theory and Its Application to Rock Engineering. *Eng Geol* 26(1):103–105
40. Shi GH, Goodman RE (1982) A new concept for support of underground and surface excavation in discontinuous rocks based on a keystone principle. *Int J Rock Mech Min Sci Geomech Abstr* 19(3):50
41. Song JJ, Lee CI (2001) Estimation of joint length distribution using window sampling. *Int J Rock Mech Min Sci* 38:519–528
42. Tang CL, Hu JC, Lin ML, Angelier J, Lu CY, Chan YC, Chu HT (2009) The Tsaoling landslide triggered by the Chi-Chi earthquake, Taiwan: insights from a discrete element simulation. *Eng Geol* 106:1–19
43. Tonon F, Chen S (2007) Closed-form and numerical solutions for the probability distribution function of fracture diameters. *Int J Rock Mech Min Sci* 44:332–350
44. Wang G, Su L, Pang JR, Sun W (2015) Research on Precision of Partial Coefficient Finite Element Method in Stability Analysis for Rock Slope. *Adv Mat Res* 1089:248–252
45. Wang HB, Zhang B, Mei G, Xu NX (2020) A statistics-based discrete element modeling method coupled with the strength reduction method for the stability analysis of jointed rock slopes. *Eng Geol* 264:105247
46. Warburton PM (1980) A stereological interpretation of joint trace data. *Int J Rock Mech Min Sci Geomech Abstr* 17:181–190
47. Wei Z, Lü Q, Sun H, Shang Y (2019) Estimating the rainfall threshold of a deep-seated landslide by integrating models for predicting the groundwater level and stability analysis of the slope. *Eng Geol* 253:14–26
48. Xu CS, Dowd P (2010) A new computer code for discrete fracture network modelling. *Comput Geosci* 36:292–301
49. Xu LM, Chen JP, Wang Q, Zhou FJ (2013) Fuzzy C-means cluster analysis based on mutative scale chaos optimization algorithm for the grouping of discontinuity sets. *Rock Mech Rock Eng* 46:189–198
50. Ye YW (2019) Simplification of discrete fracture network and application in tunnel stability analysis. Master's thesis, China University of Geosciences, Beijing
51. Zhang L (1999) Analysis and design of drilled shafts in rock. PhD thesis, Massachusetts Institute of Technology, Cambridge, MA
52. Zhang L, Einstein HH (1998) Estimating the mean trace length of rock discontinuities. *Rock Mech Rock Eng* 31:217–235
53. Zhang L, Einstein HH (2000) Estimating the intensity of rock discontinuities. *Int J Rock Mech Min Sci* 37:819–837
54. Zhang Q, Wang Q, Chen JP, Li YY, Ruan YK (2016) Estimation of mean trace length by setting scanlines in rectangular sampling window. *Int J Rock Mech Min Sci* 84:74–79
55. Zhang W, Chen JP, Cao ZX, Wang RY (2013) Size effect of RQD and generalized representative volume elements: a case study on an underground excavation in Baihetan dam, Southwest China. *Tunn Undergr Space Technol* 35:89–98
56. Zhang W, Fu R, Tan C, Ma ZF, Zhang Y, Song SY, Xu PH, Wang SN, Zhao YP (2020) Two-dimensional discrepancies in fracture geometric factors and connectivity between field-collected and stochastically modeled DFNs: a case study of sluice foundation rock mass in Datengxia, China. *Rock Mech Rock Eng* 53:2399–2417
57. Zhang W, Lan ZG, Ma ZF, Tan C, Que JS, Wang FY, Cao C (2020) Determination of statistical discontinuity persistence for a rock mass characterized by non-persistent fractures. *Int J Rock Mech Min Sci* 126:104177
58. Zheng H, Liu DF, Li CG (2005) Slope stability analysis based on elasto-plastic finite element method. *Int J Numer Methods Eng* 64:1871–1888

Publisher's Note Springer Nature remains neutral with regard to jurisdictional claims in published maps and institutional affiliations.